Orthcatter: High-throughput In-band OFDM Backscatter with Over-the-Air Code Division

Caihui Du and Jihong Yu, *Beijing Institute of Technology;*
Rongrong Zhang, *Capital Normal University;* Ju Ren, *Tsinghua University;*
Jianping An, *Beijing Institute of Technology*

https://www.usenix.org/conference/nsdi24/presentation/du

This paper is included in the
Proceedings of the 21st USENIX Symposium on
Networked Systems Design and Implementation.

April 16–18, 2024 • Santa Clara, CA, USA

978-1-939133-39-7

Open access to the Proceedings of the
21st USENIX Symposium on Networked
Systems Design and Implementation
is sponsored by

جامعة الملك عبدالله
للعلوم والتقنية
King Abdullah University of
Science and Technology

Orthcatter: High-throughput In-band OFDM Backscatter with Over-the-Air Code Division

Caihui Du
Beijing Institution of Technology

Jihong Yu *
Beijing Institution of Technology

Rongrong Zhang
Capital Normal University

Ju Ren
Tsinghua University

Jianping An
Beijing Institution of Technology

Abstract

The existing ambient backscatter systems suffer from either more spectrum utilization or low throughput. we propose Orthcatter, the first in-band OFDM backscatter system that provides a higher throughput while consuming fewer spectrum resources. Our key innovation is the designed over-the-air code division technique that enables the cancellation of the co-channel interferences, solving the core challenge of the in-band backscatter communication. Unlike the common code-division systems that generate orthogonal codewords locally, we construct the quasi-orthogonal backscatter codewords by swapping the subcarriers of each excitation OFDM symbol and concrete this design passively with a double side-band symbol construction method. Armed with these quasi-orthogonal codewords, we design a two-step interference cancellation scheme, significantly improving reliability. We prototype and test Orthcatter. The results show that Orthcatter can achieve throughput of 248kbps and a BER of 10^{-4} under OFDM WiFi exciter, improving by over 4.6× and 300× compared with the state-of-the-art in-band backscatter system. Our throughput and BER can even be 11kbps higher and 59× better than the prior side-band backscatter systems, and the exciter-to-tag communication range is 3× of prior OFDM backscatter systems.

1 Introduction

The proliferation of wireless applications brings about the ever-increasing deployments of wireless devices, which emphasizes the importance of lower power consumption and saving spectrum resources. Since ambient backscatter systems utilize the existing exciters for communication rather than requiring a dedicated carrier emitter, they are ultra-low power and play an important role in future IoT applications. Therefore, many novel backscatter systems have been proposed [7, 10, 11, 14, 19–23, 27, 29, 33–38]. Among them, the OFDM backscatter has received the most attention due to the wide deployment of OFDM exciters. Inspired by them, we envision that a ready-to-use OFDM backscatter system should satisfy the three requirements:

Table 1: Summary of OFDM backscatter systems.

Technology	High throughput	Little spectrum occupation	Single receiver
LScatter [9]	✔	✖	✖
SyncScatter [12]	✔	✖	✖
HitchHike [35]	✔	✖	✖
STScatter [33]	✔	✖	✔
RapidRider [31]	✔	✖	✖
TScatter [27]	✔	✖	✖
WiFi Backscatter [20]	✖	✔	✔
WiTAG [7]	✖	✔	✔
Study in [22] [23]	✖	✔	✔
Orthcatter	✔	✔	✔

• **High throughput.** Its data rate should be at least hundreds of kbps to support various high data rates applications such as telecommuting and live streaming.

• **Little spectrum occupation.** Due to the scarce spectrum resources, its transmission should leverage the excitation spectrum rather than occupying additional frequencies.

• **Single receiver.** It should support one-radio demodulation. That is, only one receiver is required to decode the tag data, boosting the potential for working with such popular single-receiver mobile devices as laptops and smartphones.

If these requirements were satisfied, OFDM backscatter systems could be pervasively adopted for ultra-low power communication and thus radically change our life. For example, even in smart cities with a crowded radio spectrum, backscatter devices can still provide efficient data transmission by reusing the signal and spectrum of the existing exciters. Passive wearable sensors can also interact with one-receiver devices like smartphones or smartwatches without consuming extra spectrum or power resources. Unfortunately, to our knowledge, no existing systems satisfy these requirements simultaneously (c.f. Table 1).

The reason preventing this lies in that prior works are

*Corresponding author: Jihong Yu.

forced to tradeoff between the less spectrum occupation and the higher throughput. Specifically, studies in [9, 12, 27, 31, 33, 34, 36] provide side-band backscatter systems. They show high throughput yet consuming significant spectrum resources because they must shift the backscatter signal into a new channel, referred to as the backscatter channel, to avoid the original signal. The frequency shift doubles the channel occupancy and requires an empty channel which may not exist in today's crowded wireless environment. Moreover, their backscatter receivers do not known the excitation data a priori, they have to use two physically-separated receivers and synchronize them for decoding the tag data [12, 27, 31, 34–36]. This significantly complicate their deployment and limit their usage.

Studies in [7, 11, 20, 22, 23] design in-band backscatter systems. Unlike the side-band systems, they do not frequency shift the backscatter signal, so they would not occupy extra spectrum and can decode tag data by reusing the receiver that is already deployed for the exciter's transmission. However, the backscatter signal is strongly interfered by the coexisting original signal. These works cannot eliminate such interference effectively, suffering from poor BER (over 10^{-1}) and low throughput (tens of kbps). Therefore, the existing backscatter systems transmit the tag data either in an independent backscatter channel for a higher data rate (namely side-band systems), or in the original channel with poor reliability for saving the spectrum resources (namely in-band systems).

Solving the trade-off problem, we present Orthcatter, the first **in-band** OFDM backscatter system that has a communication ability comparable to the side-band systems. Similar to prior works, Orthcatter reflects the ambient excitation signal to generate the backscatter signal and embeds every 1-bit tag data over an excitation data segment in the backscatter signal. We define such excitation data segment carrying tag data as the **backscatter codeword** and define the excitation data segment in the original signal overlapping with the backscatter codeword in the time and frequency domain as the **original codeword**. These codewords possess two features. 1) As Orthcatter transmits data at the single-symbol rate, the length of the backscatter codeword equals that of an OFDM symbol. We emphasize that the backscatter codeword is not an OFDM symbol; instead, it is constructed by combining halves of two successive OFDM symbols (c.f. §3.1). 2) Consider in-band Orthcatter, the original codeword would interfere with the backscatter codeword, posing great challenge for tag data decoding. We would make the original and backscatter codeword quasi-orthogonal during backscatter modulation and design the interference cancellation scheme in §3.2.

As shown in Figure 1, Tag in Orthcatter not only changes the phase of the backscatter codewords to embed his data but also varies their content to make them so different from the original codewords that the receiver Bob can perform interference cancellation. Our key observation is that the randomization process at the scrambler of an OFDM exciter ensures any non-overlapped data segments are non-identical. Inspired

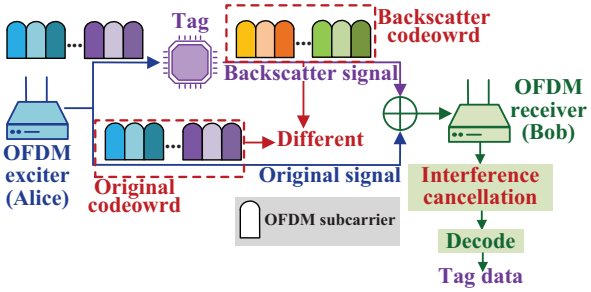

Figure 1: Concept of Orthcatter.

by this, we design the **over-the-air code division** technique which makes the original and backscatter codewords contain non-overlapping excitation data segments. This way, the correlation result between such codewords is small. We find such correlation results less than 0.5 under the 802.11g WiFi and less than 0.1 under the 20MHz LTE. Since the correlation results are not equal to 0 (i.e., orthogonal), we define the relation between our original and backscatter codewords as **quasi-orthogonal** for distinction. The quasi-orthogonality provides a chance for the receiver Bob to effectively cancel the interference from the original codewords and decode the tag data. To passively generate the backscatter codewords, we design the **double side-band symbol construction method** with a passive RF switch. During backscattering, this switch creates two OFDM symbols whose in-band parts would splice over the air into a new symbol that contains the backscatter codeword quasi-orthogonal with the original one.

In the design of Orthcatter, we answer three questions.

1) How to design the quasi-orthogonal codewords utilized for backscattering? To enable interference cancellation on the receiver side, it is crucial to ensure that the backscatter codewords are quasi-orthogonal to the original ones. This is challenging because the backscatter codewords are constructed from the uncontrolled excitation data segments rather than the Pseudo-Noise (PN) sequences that can be locally generated by conventional code-division systems. Furthermore, modifying each excitation data in the original codeword with such PN sequences to create the backscatter codeword is also not feasible. This is because Tag can only modulate the original signal in the time domain where the subcarriers carrying the excitation data would overlap. Hence, we must design the backscatter without local PN sequences.
Solution. We propose the over-the-air code division in §3.1 which makes the backscatter and original codewords quasi-orthogonal by building the former to carry non-overlapping excitation data segments with the latter. As shown in Figure 2, we generate the quasi-orthogonal backscatter codeword via two steps: subcarrier swapping and tag data mapping. In the first step, we exchange the position of the first and second half of each backscattered OFDM symbol in frequency domain. In the second step, we maps every bit of tag data into a manipulated excitation data segment. Note that we utilize the second half of a backscattered OFDM symbol and the

first half of its following one to carry every bit of tag data. This way, the original and backscatter codewords would carry non-overlapping data segments and are thus quasi-orthogonal.

2) How to passively generate the backscatter codewords? The over-the-air code division technique requires to swap frequency-domain subcarriers. However, a passive tag can only modulate the excitation signal in the time domain where the subcarriers overlap. This scheme also needs to embed the first and second half of each backscatter symbol with different tag data, requiring the modulation of the tag at the **half-symbol** level. However, the state-of-the-art works like RapidRider and STScatter [31, 33] just support single-symbol modulation for the overlapped subcarriers in the time domain.
Solution. We propose a double side-band symbol construction method in §3.1, which gets the desired backscatter OFDM symbol with a passive RF switch. This switch, toggling at fHz, can create two copies of an excitation OFDM symbol with frequency deviation of $\pm f$ from its center frequency during backscattering. We set $f = BW/2$ where BW is the bandwidth of the excitation signal so that just one half of each copy would fall inside the excitation channel and they can splice into a new OFDM symbol over the air which conveys 1-bit tag data, referred to as a backscatter symbol. This realizes the subcarrier swapping because the backscatter symbol is built by reversing the order of the first and second half of the two neighbour original excitation symbols, respectively. In addition, we vary the phase of these copies individually, making each in-band half of the copies modulated independently and achieving the half-symbol level modulation.

3) How to cope with the interference from the original signal? Since Orthcatter is an in-band system that conducts the backscatter communication in the same channel as the original one, the original signal would greatly interfere with its communication. Prior in-band works [22,23] use the redundant coding which embeds 1-bit tag data into multiple OFDM symbols or packets to cope with this interference. This significantly degrades the throughput to tens of kbps, e.g., 40kbps in [22]. In addition, their communication distance is still short, e.g., 5m in [22], because the original signal is not diminished at all and still hurts the tag data decoding. Therefore, we should cancel the interference of the original signal before decoding tag data for better decoding performance.
Solution. Given that the over-the-air code division ensures the quasi-orthogonality, we solve this through the proposed quasi-orthogonal interference cancellation and decoding scheme in §3.2. Bob can cancel the original signal via coarse and accurate cancellation. The coarse cancellation process roughly computes the original channel state from the inner product of the received OFDM symbol and the quasi-orthogonal codewords, and the accurate cancellation process adopts an adaptive filter to eliminate the residual original signal after the coarse cancellation process. Superior to prior works, most of the original signal is canceled before tag data decoding. Hence, our Orthcatter improves communication performance.

By answering these questions, we prototype Orthcatter and conduct experiments with typical OFDM exciters like WiFi and LTE. Our main results are summarized as follows.

- Orthcatter has an impressive throughput of 248kbps. It is 6.2× and 4.6× higher than the in-band backscatter systems [22] and [23], respectively. It is 11kbps higher than the side-band backscatter system RapidRider [31].
- Orthcatter's minimal BER under WiFi exciters is 3.4×10^{-4}, which is 59× and over 300× better than the side-band system RapidRider and the in-band system [23], respectively.
- Orthcatter is generic because it does not involve any upper-layer coding schemes of the exciter. It can work with different types of OFDM exciters, such as WiFi and LTE. Moreover, our tag can be put 3× further from the exciter Alice than prior OFDM backscatter works.

In summary, we design and build Orthcatter, the first in-band OFDM backscatter system that saves spectrum resources while providing considerable throughput. Our design makes the following technical contributions:

1) Over-the-air code division. This technique makes the original and backscatter codewords quasi-orthogonal. It enables the interference cancellation that is not supported in existing in-band works [22, 23].

2) Double side-band symbol construction. This method concretes the backscatter codewords and embeds tag data while keeping the power consumption similar to existing backscatter systems [27, 35, 36].

3) Quasi-orthogonal interference cancellation and decoding. This method separates the backscatter signal and the original one on the receiver side. It decodes tag data under much smaller interference, enabling better decoding performance than the state-of-the-art in-band works [22, 23].

2 Motivation and Design Overview

2.1 What makes Orthcatter outstanding?

Before introducing our Orthcatter, we first show what makes it outstanding. To explain this, we classify the current OFDM backscatter systems into two types: side-band and in-band. Tags in side-band backscatter systems would frequency shift the backscatter signal to another channel to avoid the original signal [12, 27, 31, 33, 35, 36]. Since the original signal would not interfere with backscatter transmission, they provide high throughput, e.g., hundreds of kbps, and good BER performance, e.g., around 10^{-3}. However, they share some severe drawbacks: **1) Large spectrum resources occupation.** The frequency shift here consumes significant spectrum resources, e.g., 20MHz under OFDM WiFi exciter. **2) Vulnerable transmission.** Since a tag cannot sense or occupy an empty channel for communication, the transmission suffers from strong interference in today's crowded wireless environment. **3) Complex deployment.** Most of these works [12, 27, 31, 35, 36] have to use and synchronize two physically-separated receivers since

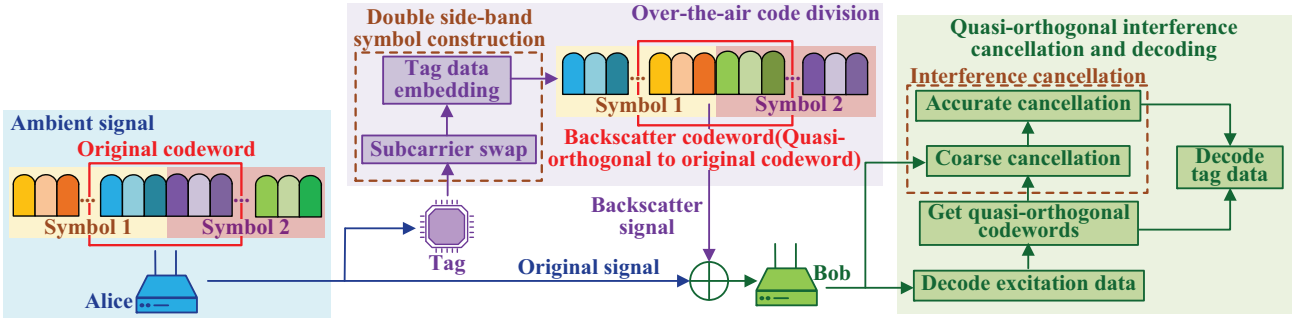

Figure 2: Orthcatter overview. Symbols 1 and 2 are two OFDM symbols, the backscatter codeword carrying 1-bit tag data is built from two excitation symbols by Tag. It is interfered by the original codeword.

they need to receive the original and backscatter signals in two frequency channels for decoding tag data.

Tags in the in-band backscatter systems transmit his data in the original channel [7,20,22,23]. These works saves the spectrum resources and can get tag data by reusing the receiver deployed for Alice's transmission. Moreover, other ambient signals would not interfere with their transmission because commercial systems can occupy the wireless channel through channel access methods like RTS/CTS scheme [13]. However, the received signal is a superposition of the original and backscatter signals. Worse still, the receiver cannot cancel the original signal effectively. To address this problem, redundant coding is used to make the superposed signal decodable on the receiver side. WiFi Backscatter [20] and WiTag [7] embeds 1-bit tag data over a WiFi frame with tens of OFDM symbols. Both [22] and [23] encode 1-bit tag data over multiple OFDM symbols. Unfortunately, they still experience poor BER. For example, although [23] encodes 1-bit tag data over four WiFi symbols (16 μs), its minimal BER is over 10^{-1}.

Observation. We observe that the root cause preventing the interference cancellation is the extreme similarity between the received original signal and the backscatter signal. For example, a received OFDM symbol Y_r in [23] is

$$Y_r = Y_o + Y_b = \sum_{i=1}^{N} H_o(i) S_i e^{-j2\pi f_i t} + \sum_{i=1}^{N} H_b(i) B S_i e^{-j2\pi f_i t} \quad (1)$$

where Y_o is the original symbol, Y_b is the backscatter symbol, N is the number of subcarriers in a symbol, and B is the tag data. Consider the i-th subcarrier, S_i is its excitation data, f_i is its center frequency, $H_o(i)$ is the direct-link channel state, and $H_b(i)$ is the backscatter channel state.

The differences between Y_o and Y_b just lie in the channel state and an initial phase offset that exists only when the transmitted tag data is '1'. Consequently, the receiver cannot distinguish Y_o and Y_b, and has to decode with strong interference. Denote by $S = \{S_i, \cdots, S_N\}$ the data carried by the original codeword, the observation inspires us to design Orthcatter that enables interference cancellation by making Y_o and Y_b carry different S. The problem hindering our design is whether we can achieve this without consuming extra power. Our answer is YES, and our insight is that two non-overlapping excitation data segments would be quasi-orthogonal thanks to the scrambler at the OFDM exciter. Specifically, we make Y_b carry the backscatter codeword that is quasi-orthogonal to the original codeword carried by Y_o (c.f. Figure 2). Y_r here hence becomes

$$Y_r = Y_o + Y_b = \sum_{i=1}^{N} H_o(i) S_i e^{-j2\pi f_i t} + H_b(i) B \hat{S}_i e^{-j2\pi f_i t} \quad (2)$$

where $\hat{S}_i$ is the excitation data carried by the i-th subcarrier in the backscatter symbol. Since the backscatter codeword $\hat{S} = \{\hat{S}_1, \cdots, \hat{S}_N\}$ and S are quasi-orthogonal, Bob can separate Y_o and Y_b, and decodes tag data under much smaller interference. Therefore, Orthcatter achieves better performance.

2.2 What is Orthcatter?

Orthcatter is an in-band OFDM backscatter system that outperforms the prior works. We first give a brief description of the architecture of OFDM technology. Communication systems like WiFi and LTE utilize OFDM to embed their data into different subcarriers. For simplicity, we denote an OFDM symbol by $S = \sum_{i=1}^{N} S_i e^{-j2\pi f_i t}$ where f_i is the frequency of the subcarrier i and S_i is the carried excitation data. A scrambler would randomize S_i to avoid the all-zero or all-one sequences. That said, two segments of S_i would be nonidentical if they do not overlap. We refer to such feature as quasi-orthogonal and employ it to design Orthcatter. As shown in Figure 2, Orthcatter has three parts: Alice, Tag, and Bob.

- **Alice.** Alice is an OFDM-based exciter and is beyond control. In our experiments, we choose two typical OFDM exciters for Alice: 802.11g WiFi [6], and LTE [4].
- **Tag.** Tag could piggyback his data over the ambient OFDM excitation signals. He can naturally support generic OFDM exciters including WiFi and LTE without hardware modification. During transmission, Tag adopts the over-the-air code division technique (c.f. §3.1) which embeds and spreads his data with quasi-orthogonal backscatter codewords. As shown in Figure 2, the backscatter codeword conveys 1-bit tag data and is quasi-orthogonal to its counterpart in the original excitation signal, i.e., the original codeword in Figure

2. Such a backscatter codeword is generated passively with the double side-band symbol construction method. Through this design, Tag can embed his data at the single-symbol rate same as existing side-band systems like RapidRider [31] and thus has an impressive throughput. We emphasize that: 1) As an in-band backscatter system, Tag's transmission takes place in the same channel as the excitation signal. 2) Tag is passive with around $63.3\mu W$ power consumption (c.f.§4).

• **Bob.** Bob is an OFDM receiver that decomposes the incoming signal into frequency-domain OFDM symbols through FFT. He decodes the excitation and tag data from this symbol through the quasi-orthogonal interference cancellation and decoding method explained in §3.2. To achieve this for a strong or weak backscatter signal, he would roughly compute the ratio between the original and backscatter signal strength, and uses a ratio-aware scheme to decode the excitation data. He then eliminates the original signal through a two-step cancellation process and decodes tag data. Bob needs only **one** receiver staying at the original excitation channel.

Benefits. Orthcatter enables tag data transmission over ambient OFDM signals with two main advantages: 1) Tag data is transmitted while being decoded in the same channel as the original excitation signal with only one receiver needed. 2) Interference from the excitation signal is cancelled. With these advantages, Orthcatter has the potential to be deployed in noisy and signal-rich environments like office buildings and smart cities. Orthcatter achieves even better throughput and BER than the state-of-the-art side-band backscatter system like RapidRider [31], meaning that it consumes few spectrum resources without harming the communication ability. We believe that our design benefits a wide range of applications.

3 Design

3.1 Encoding: Over-the-air code division

As shown in Figure 2, we construct the backscatter codeword from two adjacent excitation OFDM symbols, i.e., symbols 1 and 2, and utilize its quasi-orthogonality with the original codeword to achieve reliable in-band backscatter communication. To enable this, we design the over-the-air code division technique. We first introduce the challenges in our design.

Challenges. Facing the signal collision problem, the traditional systems would carefully design their transmitted codewords for signal separation. For instance, the CDMA [30] system spreads their messages with orthogonal codewords so that the receiver can decode them independently. [25] introduces structured permutation when generating its transmitted codewords and utilizes the data carried by the collision-free subcarriers to infer the data carried by the collided subcarriers. That said, it works only when two channels partially overlap. These schemes cannot be applied directly to in-band backscatter systems for two reasons.

1) Tag cannot build the quasi-orthogonal codeword by utilizing the PN sequence to spread tag data like existing CDMA systems. In a generic backscatter system, the tag data is spread by the uncontrolled excitation data instead of the locally generated PN sequences adopted by existing CDMA systems. If Tag tries to modulate the excitation data with a PN sequence, it would modulate all the excitation data in one OFDM symbol instead of any individual one [33]. For instance, denote the phase shift to convey data in the PN sequnece by $e^{j\phi_t}$ and an OFDM symbol by $S = \{S_1, S_2, \ldots, S_N\}$. Embedding this data via backscatter yields the symbol $\hat{S} = \{S_1 e^{j\phi_t}, S_2 e^{j\phi_t}, \ldots, S_N e^{j\phi_t}\}$ instead of the desired $\{S_1 e^{j\phi_t}, S_2, \ldots, S_N\}$. Here the value of the normalized correlation result between S and $\hat{S}$ is still one, and the quasi-orthogonality is not established.

2) Constructing the desired quasi-orthogonal codewords must consume similar power as prior backscatter systems. As shown in Figure 2, generating the backscatter codeword requires changing the subcarrier pattern and modulating at the half-symbol level. This causes trouble because excitation data of an OFDM symbol are independent in the frequency domain and coexist in the time domain. However, without energy-consuming components like ADCs and mixers, Tag cannot convert his received time-domain signal to the frequency domain to manipulate the excitation codewords individually. Hence, we must keep time-domain modulation while changing the subcarrier pattern to generate the desired backscatter codewords without rising energy consumption.

Solutions: over-the-air code division. Recall that an excitation data segment that is embedded with 1-bit tag data is called a backscatter codeword, we aim at making it quasi-orthogonal to its counterpart in the original excitation signal, i.e., the original codeword. To this end, we design the over-the-air code division technique, which builds quasi-orthogonal codewords without relying on local PN sequences. As shown in Figure 3, this method makes the original and backscatter codewords carry non-overlapping excitation data segments. This way, since the randomization at Alice ensures that two non-overlapping data segments are different, the original and backscatter codewords are quasi-orthogonal. Specifically, the backscatter codeword is built by two steps: subcarrier swapping and tag data mapping.

To explain this, we take the symbol 1 (denoted as $S1$) and symbol 2 (denoted as $S2$) as an example, each containing N subcarriers which are denoted by $S1_1 \sim S1_N$ and $S2_1 \sim S2_N$, respectively. **In the subcarrier swapping step**, Tag reverses the order of the first and second half of each OFDM symbol. This changes $S1$ and $S2$ into the backscatter symbols $\hat{S1} = \{S1_{N/2+1} \cdots S1_N, S1_1 \cdots S1_{N/2}\}$ and $\hat{S2} = \{S2_{N/2+1} \cdots S2_N, S2_1 \cdots S2_{N/2}\}$. **In the tag data mapping step**, he pieces the second half of $\hat{S1}$, i.e., $S1_{N/2+1} \sim S1_N$, and the first half of $\hat{S2}$, i.e., $S2_{N/2+1} \sim S2_N$, to form the backscatter codeword $\{S1_1 \ldots S1_{N/2}, S2_{N/2+1} \ldots S2_N\}$ conveying 1-bit tag data, i.e., the backscatter codeword in Figure 3. This is completely different from prior works [31, 35, 36] that em-

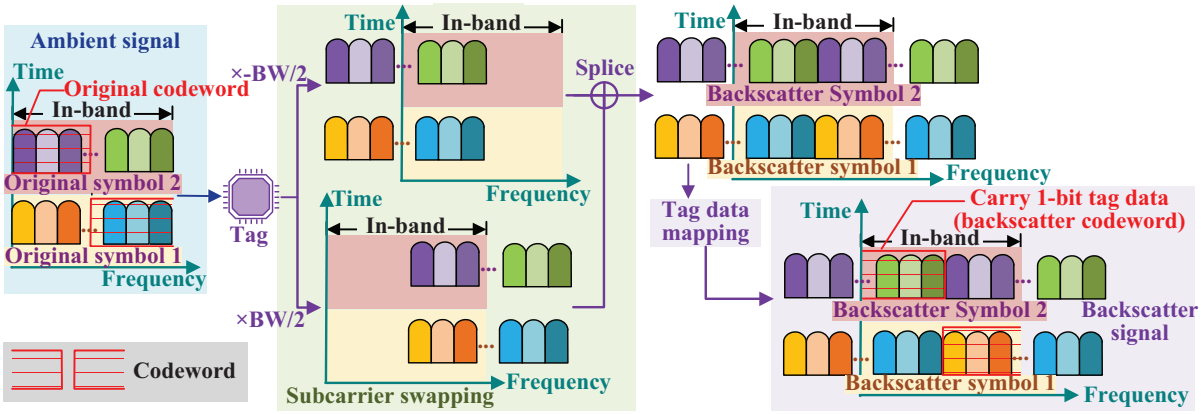

Figure 3: Overview of the over-the-air code division. The backscatter codeword carries 1-bit tag data and is interfered with by the original codeword. We make them quasi-orthogonal for interference cancellation.

beds 1-bit data over the whole $S1$ or $S2$. This way, the original codeword coexisting with such backscatter codeword is $\{S1_{N/2+1}\dots S1_N, S2_1\dots S2_{N/2}\}$. They are made from non-overlapping excitation data and hence are quasi-orthogonal. Note that the rest of the in-band subcarriers, i.e., $S1_{N/2+1}\sim S1_N$ and $S2_{N/2+1}\sim S2_N$, would not be wasted, they are also utilized to form other quasi-orthogonal codewords. Specifically, $S1_{N/2+1}\sim S1_N$ is pieced with the second half of the preceding backscatter symbol and $S2_{N/2+1}\sim S2_N$ is pieced with the first half of the backscatter symbol following $\hat{S}2$.

We emphasize that these backscatter symbols $\hat{S}_1$ and $\hat{S}_2$ would hardly be affected by the impact brought by propagation delays, echoes, and reflections. The reason is that the time domain guard signal, i.e., CP, in an OFDM system is utilized to add immunity to these effects. During our generation process, the tag would change the CP and the data part of an OFDM symbol based on the same scheme and tag data, making it still hold that the CP is the same as the end of the OFDM backscatter symbol, that said, the receiver still receives the backscatter codeword $S_b=\{S1_{N/2+1}\dots S1_N, S2_1\dots S2_{N/2}\}$.

Passive quasi-orthogonal codeword generation. The key left is to arm a tag with the ability of modulating subcarriers of an OFDM symbol, i.e., conducting half-symbol level modulation. To this end, Orthcatter leverages the fact that an fHz square wave generated by the tag can shift the original signal by $\pm f$Hz during backscattering. Such a double side-band characteristic is unwanted in prior side-band backscatter systems because it introduces interference in the adjacent channels. In contrast, we turn it into profits and design the **double side-band symbol reconstruction** method, which passively builds the backscatter codeword. Specifically, Tag adopts a passive switch and toggles it at $f=BW/2$ to create the square wave. As shown in Figure 3, this square wave shifts the original OFDM symbols $S1$ and $S2$ by $\pm BW/2$. This way, the in-band parts of these frequency-shift subcarriers would splice over the air forming the backscatter OFDM symbols $\hat{S}_1$ and $\hat{S}_2$. Since $S1$ and $S2$ are shifted by the same process, we take $S1$ as an example to explain this in details. Suppose Tag toggles the switch at $f_t=BW/2$, his antenna reflection coefficient $\Gamma(t)$ would be changed following a square wave $y_t(t)$. From the Fourier analysis [17], $y_t(t)$ is

$$\begin{aligned} y_t(t) &= \frac{4}{\pi}\sum_{n=1}^{\infty}\frac{\bar{\Gamma}\sin\left((2n-1)2\pi f_t t\right)}{2n-1} \\ &\approx \frac{4\bar{\Gamma}}{\pi}\sin(2\pi f_t t) = \frac{2j\bar{\Gamma}}{\pi}\left(e^{-j2\pi f_t t}-e^{j2\pi f_t t}\right) \end{aligned} \tag{3}$$

where $\bar{\Gamma}$ denotes the amplitude and phase of $\Gamma(t)$. For example, $\bar{\Gamma}=j$ when Tag alters $\Gamma(t)$ between $\pm j$.

Let f_c and $y_b(t)$ respectively be the OFDM excitation signal's center frequency and baseband waveform. The backscatter signal output from the switch is

$$\begin{aligned} y_{out}(t) &= A_1 y_b(t) e^{-j2\pi f_c t} y_t(t) \\ &= \frac{2A_1 y_b(t)\bar{\Gamma} j}{\pi}\left(e^{-j2\pi(f_c+f_t)t}-e^{-j2\pi(f_c-f_t)t}\right) \end{aligned} \tag{4}$$

where A_1 is the antenna gain. This equation shows that the in-band subcarriers of $y_{out}(t)$ is $\{S1_{N/2+1}\dots S1_N, S1_1\dots S1_{N/2}\}$, which is the desired backscatter OFDM symbol $\hat{S}_1$. Consequently, we passively achieve the subcarrier swapping. After this, Tag should embed his data over the built quasi-orthogonal codewords, e.g., the backscatter codeword in Figure 3. This requires embedding different tag data over the first and second half of $\hat{S}1$ because they belong to the different backscatter codewords. That said, Tag needs to take two adjacent data during modulation and change the phases of the subcarriers at a time. $\hat{S}1$ after embedding tag data (td) is

$$\hat{S}1=\begin{cases}\{S1_{N/2+1},\dots,S1_N,S1_1,\dots,S1_{N/2}\}, & td=\{0,0\}\\ \{-S1_{N/2+1},\dots,-S1_N,S1_1,\dots,S1_{N/2}\}, & td=\{1,0\}\\ \{S1_{N/2+1},\dots,S1_N,-S1_1,\dots,-S1_{N/2}\}, & td=\{0,1\}\\ \{-S1_{N/2+1},\dots,-S1_N,-S1_1,\dots,-S1_{N/2}\}, & td=\{1,1\}\end{cases} \tag{5}$$

This indicates that the modulation is performed at the **half-symbol level**. In traditional backscatter systems, this is

unattainable because the subcarriers are inseparable in the time domain where a passive tag conducts his modulation [33]. In contrast, our tag would create two copies of backscatter signals at two side-bands, whose in-band parts form the backscatter symbol. Employing such double side-band nature, we can thus modulate the first and second half of the backscatter symbol individually. To further explain this, we distinguish (5) into two cases based on whether the phases of the first and second half of $\hat{S}1$ are opposite.

• **Case 1: Tag data is $\{1,0\}$ or $\{0,1\}$.** Recall (5), the phases of the first and second half of $\hat{S}1$ are opposite, so we alter $\Gamma(t)$ between $\pm j$ to transmit these tag data. We consider an antenna with impedance $Z_A = 50$. Since $\Gamma(t) = \frac{Z_L(t)-Z_A}{Z_L(t)+Z_A}$, altering the load impedance $Z_L(t)$ between $\pm j50$ could change $\Gamma(t)$. The output signal $y_{out1}(t)$ is shown in (6), and we reverse it for tag data of $\{1,0\}$ and do nothing for $\{0,1\}$.

$$y_{out1}(t) = \frac{2A_1 y_b(t)}{\pi}\left(-e^{-j2\pi(f_c+f_t)t} + e^{-j2\pi(f_c-f_t)t}\right) \quad (6)$$

• **Case 2: Tag data is $\{1,1\}$ or $\{0,0\}$.** The phases of the first and second half of these subcarriers are identical, making $y_t(t)$ in Case 1 unsuitable. We here delay $y_t(t)$ by $\frac{f_t}{4}$ to create an additional $\pi/2$ phase offset, reformulating (3) into

$$\begin{aligned} y_t(t) &= \frac{2j\bar{\Gamma}}{\pi}\left(e^{-j2\pi f_t(t-\frac{1}{4f_t})} - e^{j2\pi f_t(t-\frac{1}{4f_t})}\right) \\ &= -\frac{2\bar{\Gamma}}{\pi}\left(e^{-j2\pi f_t t} + e^{j2\pi f_t t}\right) \end{aligned} \quad (7)$$

We change the load impedance $Z_L(t)$ between 0 and $+\infty$ to alter $\Gamma(t)$ between ± 1 and transmit the tag data. Such $y_{out}(t)$ is stated in (8) and is reversed when tag data is $\{0,0\}$.

$$y_{out}(t) = \frac{-2A_1}{\pi}\left(e^{-j2\pi(f_c+f_t)t} + e^{-j2\pi(f_c-f_t)t}\right) \quad (8)$$

As analysed above, we change $Z_L(t)$ among $\pm j50$, 0 and $+\infty$ to get (5), which enables the half-symbol level modulation. Compared with the prior works [27, 31, 35, 36] that changes $Z_L(t)$ between 0 and $+\infty$, our $Z_L(t)$ has two additional values. This would hardly increase the hardware complexity or the power consumption because we only need to arm Tag with a passive RF switch that has more states. As confirmed in §4, such a passive RF switch has a less than 3.3μW power consumption which is similar to the power consumption of the RF switch adopted by the prior backscatter works [32].

3.2 Decoding: Quasi-orthogonal interference cancellation

We have presented how to generate the backscatter signal carrying the quasi-orthogonal backscatter codewords where tag data are embedded. Here we focus on decoding the tag data at Bob. As illustrated in Figure 2, we need the quasi-orthogonal codewords to perform interference cancellation and get tag data. To this end, we first decode the excitation data from the received superposition signal. Specifically, we would roughly compute the signal strength ratio. If the excitation signal is 10dB stronger than the backscatter one, we employ the capture effect to decode it. Otherwise, we utilize the null subcarriers to create the linear equations with a unique solution and decode the excitation data by solving these equations. Second, we infer the quasi-orthogonal codewords and conduct a two-step interference cancellation scheme to extract the backscatter signal. In the step 1, we regard the original channel state as constant among different subcarriers and roughly subtract the extracted excitation signal from the received one. In the step 2, we utilize the adaptive filter to further eliminate the residual excitation signal, and decode tag data from the left signal. Our decoding process is detailed as follows.

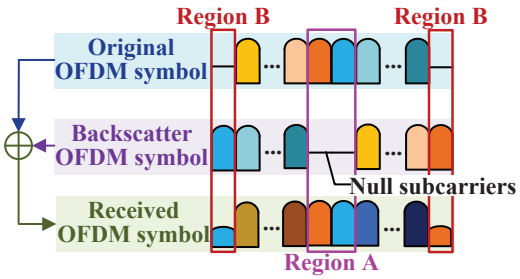

Figure 4: Illustration of the received OFDM symbol. Region A contains only the original excitation OFDM subcarriers and Region B contains only the backscatter OFDM subcarriers due to the existence of null subcarriers.

Decoding the excitation data. We need to decode the excitation data first to infer the quasi-orthogonal codewords. Since the original signal is much stronger than the backscatter one, we decode the excitation data from it based on the capture effect. However, such decoding would result in a higher BER unless the original signal is 10dB higher than the backscatter one [24]. That said, to get the excitation data correctly, Bob must first sense the ratio of the excitation signal strength to the backscatter one before employing the capture effect.

We achieve this through an empty part of the OFDM spectrum, i.e., the null subcarriers. These subcarriers usually lie on the sides of an OFDM symbol spectrum as the frequency-domain guard interval. However, these subcarriers would be moved to to the center of the backscatter symbol by the over-the-air code division scheme. This makes some subcarriers in the received OFDM symbol come from either the original or backscatter symbol, which can be utilized for computing the signal strength ratio. As shown in Figure 4, the received subcarriers in Region A only come from the original OFDM symbol, and those in Region B are only from the backscatter OFDM symbol. Therefore, we calculate the original and backscatter signal strength from the subcarriers strength in these regions. If the original subcarriers is 10dB stronger than the backscatter ones, we adopt the capture effect to get the excitation data; otherwise, we design the following ap-

proach. Take the OFDM symbol $S1$ as an example. Denote the received symbol of $S1$ by $\tilde{S1}$

$$\tilde{S1} = h_o S1 + h_b \hat{S1} \tag{9}$$

where h_o and h_b mean the original and backscatter channel, and $S1$ and $\hat{S1}$ are the corresponding symbols. Consider all the subcarriers, we have

$$\begin{bmatrix} \tilde{S1}_1 \\ \tilde{S1}_2 \\ \vdots \\ \tilde{S1}_N \end{bmatrix} = h_o \begin{bmatrix} S1_1 \\ S1_2 \\ \vdots \\ S1_N \end{bmatrix} + h_b \begin{bmatrix} e^{j\phi_{1t}} S1_{N/2+1} \\ \vdots \\ e^{j\phi_{1t}} S1_N \\ e^{j\phi_{2t}} S1_1 \\ \vdots \\ e^{j\phi_{2t}} S1_{N/2} \end{bmatrix} \tag{10}$$

where ϕ_{1t} and ϕ_{2t} are the phase offsets carrying different tag data. We take a deeper look at (10). It has N equations and less than N variables because the pilot and null subcarriers would make some among $S1_1 \sim S1_N$ known a priori. For example, an 802.11g WiFi symbol has 4 pilot and 12 null subcarriers, i.e., solving 52 variables in (10) with 64 equations. Therefore, it has a unique solution and we can solve it to get the channel states, i.e., h_o and h_b, and the excitation data. In this way, we get the excitation data under either strong or weak backscatter signals. We can exam this decoding result through the check code like cyclic redundancy check (CRC) adopted by the exciter. The task here hence moves to decode tag data.

Decoding the tag data. Since the quasi-orthogonal codewords are inferred after decoding the excitation data, Bob tends to decode the tag data from the inner product of the received OFDM symbol and the quasi-orthogonal codewords. There are still two problems to be solved. First, unlike the standard CDMA systems whose received signals from different transmitters have similar strength, our backscatter signal here is much weaker than the original one. Second, the relation between the original and backscatter codewords is quasi-orthogonal instead of orthogonal, meaning that the inner product between these codewords would not be zero. Consequently, the original signal greatly interferes with decoding the tag data. To address these problems, we design a two-step interference cancellation scheme. Our goal is to compute the original channel state h_o and subtract $h_o S1$ from $\tilde{S1}$.

1) Coarse cancellation. To this end, we first assume that h_o in (9) is constant across different subcarriers to compute its rough value. Specifically, Bob computes the normalized inner product among $\tilde{S1}$, $S1$, and $\hat{S1}$, and gets

$$\begin{aligned} \sum_{i=1}^{N} \frac{\tilde{S1}_i S1_i^*}{|\tilde{S1}_i||S1_i|} =& N h_o + h_b e^{j\phi_{1t}} \sum_{i=1}^{N/2} \frac{S1_{N/2+i} S1_i^*}{|S1_{N/2+i}||S1_i|} \\ &+ h_b e^{\phi_{2t}} \sum_{i=1}^{N/2} \frac{S1_i S1_{N/2+i}^*}{|S1_i||S1_{N/2+i}|} \end{aligned} \tag{11}$$

$$\sum_{i=1}^{N/2} \frac{\tilde{S1}_i S1_{N/2+i}^*}{|\tilde{S1}_i||S1_{N/2+i}|} = h_o \sum_{i=1}^{N/2} \frac{S1_i S1_{N/2+i}^*}{|S1_i||S1_{N/2+i}|} + \frac{N}{2} h_b e^{j\phi_{1t}} \tag{12}$$

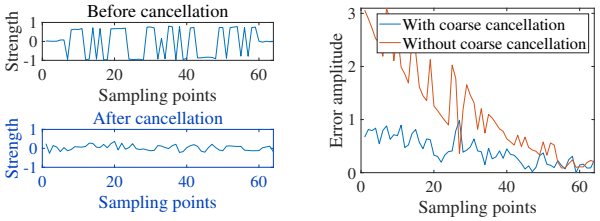

(a) Received OFDM symbol (b) Adaptive filter's convergence time

Figure 5: Empirically measured convergence time and interference cancellation performance.

$$\sum_{i=1}^{N/2} \frac{\tilde{S1}_{N/2+i} S1_i^*}{|\tilde{S1}_{N/2+i}||S1_i|} = h_o \sum_{i=1}^{N/2} \frac{S1_{N/2+i} S1_i^*}{|S1_{N/2+i}||S1_i|} + \frac{N}{2} h_b e^{j\phi_{2t}} \tag{13}$$

where $S1_i^*$ is the complex conjugate of $S1_i$.

Solving these equations yields the h_o under the hypothesis that it remains constant among different subcarriers. However, the frequency selective fading resulting from the multi-path effect would break such hypothesis. For distinction, we denote such computed h_o as $\hat{h}_o$. Since subtracting $\hat{h}_o S1$ from the received symbol $\tilde{S1}$ cannot remove all the original excitation symbol, we further conduct the accurate cancellation process.

2) Accurate cancellation. In this process, we adopt the adaptive filtering algorithm to output the remaining $S1$ after the coarse cancellation [18]. Specifically, given that the backscatter codewords are quasi-orthogonal to the original ones, we regard them as noise and utilize the least-mean-square (LMS) adaptive filter to reconstruct the remained $S1$ in $\tilde{S1}$. Denote that $\bar{S1} = \tilde{S1} - S_1 \hat{h}_o$, the LMS filter is

$$\begin{aligned} e(n) &= d(n) - \omega^H(n) u(n) \\ \omega(n+1) &= \omega(n) + \mu u(n) e^*(n) \end{aligned} \tag{14}$$

where $u(n) = S1_n/|S1_n|$ is the input variable, $d(n) = \bar{S1}_n/|S1_n|$ is the optimal output, $\omega(n)$ is the LMS filter, and $e(n)$ is the estimation error with $n = 1, 2, \ldots N$. μ is the step size not smaller than $2/R$, and R equals the square root of the self-correlation of the input variable $u(n)$.

Since $u(n)$ is very limited, e.g., 64 when the excitation signal follows 802.11g WiFi, we set μ to its maximum value for a shorter convergence time. We further subtract the output from $\bar{S1}$ to decrease the interference caused by the residual original signal. As shown in Figure 5(a), the original signal is eliminated after our two-step interference cancellation.

Although the LMS filter can distinct the original symbol from the received superposition one, we emphasize that the coarse cancellation is still necessary because the adaptive filter would waste sampling points before convergence [18]. This can be ignored in common wireless systems where the received signal with countless sampling points is input into the filter. In contrast, in our Orthcatter where the input signal is an OFDM symbol with limited sampling points, such a waste would greatly degrade the performance and hence

should be avoided. The empirically measured convergence time is shown in Figure 5(b), confirming that the coarse cancellation process significantly reduces the error and decreases the number of required sampling points.

We then decode the tag data by correlating the left signal after the interference cancellation with the inferred backscatter codeword. Since each backscatter codeword crosses two OFDM symbols, we take two OFDM symbols $S1$ and $S2$ to explain this. According to the modulation scheme, the halves of the received symbols containing a 1-bit tag data is $\check{S} = \{\check{S}1_{N/2+1}, \ldots, \check{S}1_N, \check{S}2_1, \ldots, \check{S}2_{N/2}\} \approx e^{j\phi_{2t}} h_b \{S1_1, \ldots, S1_{N/2}, S2_{N/2+1}, \ldots, S2_N\}$, and the backscatter codeword is $S_b = \{S1_1, \ldots, S1_{N/2}, S2_{N/2+1}, \ldots, S2_N\}$. Therefore, the inner product between $\check{S}$ and S_b is

$$Z_i = \left(\sum_{i=1}^{N/2} \frac{\check{S}1_{i+N/2} S1_i^*}{|\check{S}1_{i+N/2}||S1_i|} + \sum_{i=1}^{N/2} \frac{\check{S}2_i S2_{i+N/2}^*}{|\check{S}2_i||S2_{i+N/2}|} \right) = e^{j\phi_{2t}} h_b N$$

Since the phase of Z_i is $\arctan\left(\frac{h_b N \sin\phi_{2t}}{h_b N \cos\phi_{2t}}\right) = \phi_{2t}$, Bob finally decodes tag data from the phase of Z_i. The operations above benefit our Orthcatter in two ways: First, it decodes tag data under a much smaller interference, improving the throughput and communication distance. Second, since $|Z_i|$ is the sum of all the subcarrier amplitudes, it is distinguishable under a small SNR. Consequently, Orthcatter has an even smaller BER than side-band systems as confirmed in §5.

4 Orthcatter Implementation

Challenge & solution. Synchronization accuracy poses great challenge for OFDM backscatter. Specifically, in the backscatter systems that adopts a dedicated single-tone RF source as their exciter, the synchronization with the excitation signal is not required, so they achieves a further Alice-to-Tag distance, e.g., 20m in RF-transformer [14] and 9m in DigiScatter [39]. In contrast, in the OFDM backscatter systems, Tag must achieve symbol synchronization because his data is transmitted at the single-symbol rate for higher throughput [12]. Consequently, most of them [9, 27, 28, 31, 37] maintain Alice-to-Tag distance within 1m for better BER. Consider such limitation, we try to break it in Orthcatter.

The prior works usually utilize an envelope average and a comparator to determine whether tag receives the ambient OFDM signal and hence synchronize tag's transmission with this signal [37]. While such an energy detection method shows a small power consumption, it has a very limited synchronization distance because it cannot detect the weak signal. To address this limitation, we propose a matching scheme instead of the energy detection method used in works [9, 27, 28, 31, 37] to detect the weaker ambient OFDM signal.

Our **sliding window matching** scheme (c.f. Figure 6) enhances synchronization with the cyclic prefix (CP) of an OFDM symbol. Given that the CP is a periodic extension

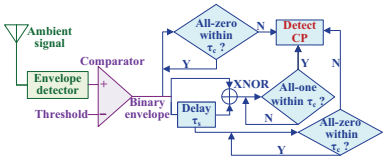

Figure 6: The sliding window matching scheme.

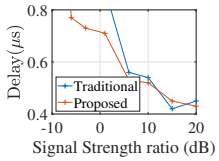

Figure 7: Delay of synchronization.

of the OFDM symbol, it holds that $y(t) = y(t+\tau_s), t \in [0, \tau_c]$ where τ_c and τ_s are the duration of the CP and the data part of an OFDM symbol, respectively. Our basic idea is to use a sliding window that matches every τ_c of the OFDM signal with the OFDM signal delayed by τ_s. As shown in Figure 6, we would first utilize an envelope detector to extract the envelope of the OFDM signal and then utilize a comparator with a predetermined threshold to binarize the envelope. We divide the binary envelope sequence into two paths and delay one path by τ_s. Finally, we compute the XNOR result between these paths which would remain one for τ_c if the CP is detected or the noise keeps below the threshold. Therefore, if the XNOR result remains one within τ_c while neither of these sequences is all-zero, the CP is detected and Tag can synchronize with the excitation signal. Note that we set the threshold to 1V based on the empirically measured noise floor.

To show the advantage of this scheme, we test the synchronization accuracy under 802.11g WiFi exciter. We put Alice 0.1m away from Tag. As shown in Figure. 7, When the excitation signal strength is over 1dBm, our approach and the traditional one has similar synchronization accuracy. This is because we digitize the ambient signal's envelope with the same approach as the traditional one. When the signal strength drops below -6dBm, our approach maintains a synchronization accuracy within 750ns while the traditional approach fail to detect the ambient signal. Different from the traditional 1-bit detection scheme, our approach is a correlation-based synchronization scheme that considers multiple bits of the digitized envelope sequence at a time and thereby achieves synchronization under weaker signals. Therefore, our proposed scheme enables accurate synchronization within a longer distance. The experiment results in §5 confirm this.

Backscatter tag. We implement Orthcatter following an open-source backscatter platform [32] that is widely used [9, 27, 35, 36] (c.f. Figure 8(a)). The power consumption of its simulated ASIC design is merely 33μW. However, due to the high tap out cost, it utilizes COTS components to build its hardware prototype, resulting in power consumption of 40mW. The increased power consumption mainly results from the utilization of an FPGA and a COTS envelope detector LT5534 [3]. Both of these components consumes tens of microwatts energy. We only replace the SPST ADG902 RF switch [1] with an SP4T ADG904 RF switch [2] to get the required antenna coefficient for generating the quasi-orthogonal

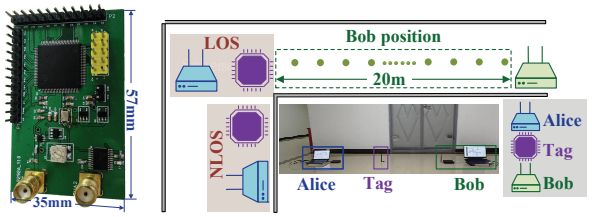

(a) Tag prototype (b) LOS & NLOS experiment setup

Figure 8: Tag prototype and experiment setup.

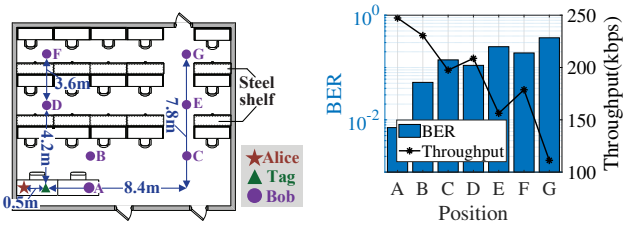

(a) Deployment (b) Performance

Figure 9: Testing Orthcatter in laboratory.

codewords. According to the data sheets, these two types of RF switches have the same maximum quiescent power supply current of 1μA under the 3.3V voltage supply. Therefore, our prototype also has about 40mW power consumption. By conducting ASIC design, the modulation component of Orthscatter has 56μW power consumption, and the detection component implemented by LT5534 is passive, so the simulated overall power consumption of Orthscatter is 63.3μW.

Alice & Bob. We adopt two USRPs for Alice and Bob, and choose two typical commercial OFDM signals as exciters: 802.11g WiFi and LTE. The WiFi signal is implemented with the open-source 802.11g WiFi transceiver on Ubuntu [8]. The LTE signal is generated on MATLAB by the LTE toolbox [5]. They are compatible with the commercial standards [8] [5].

5 Orthcatter Evaluation

We evaluate Orthcatter's performance under diverse scenarios. Our experiment confirms that it outperforms the state-of-the-art in-band backscatter systems [22, 23] in terms of BER, throughput, and communication distance. 1) The maximal throughput of Orthcatter is 248kbps, which is 6.2× higher than [22], and 4.6× higher than [23]. 2) The minimal BER of Orthcatter under WiFi is 3.4×10^{-4}, which is over 300× better than [23]. 3) When the communication distance is 20m, the throughput of [22] and [23] drops to zero, yet Orthcatter still experiences throughput of over 50kbps. Orthcatter also outperforms the side-band backscatter system like RapidRider [31]. Under the same settings, Orthcatter increases the maximum throughput by 11kbps and reduces the minimal BER by 59×.

5.1 Experiment Setup

Settings. As shown in Figure 8(b), we test Orthcatter in the LOS and NLOS scenarios. We use an 802.11g OFDM WiFi exciter. The packet rate is 500pkt/s, and the transmit power equals the common value of WiFi products, i.e., 20dBm [16].

Competitions. We compare Orthcatter with in-band [22, 23] and side-band OFDM backscatter systems [31]. Specifically, we choose RapidRider to signify the state-of-the-art side-band OFDM backscatter system. This work is known for its throughput and symbol-level modulation. However, it needs two receivers deployed in the original and backscatter channels respectively, occupying more spectrum resources. [22, 23] are in-band OFDM backscatter systems and have to use redundant coding schemes to cope with the interference caused by the excitation signal. Consequently, they show much lower throughput and a much worse BER.

5.2 End-to-End Performance

We set the Alice-to-Tag distance same as RapidRider and [23], i.e, 0.5m and 1m, and choose the same type of the exciter. We vary the Tag-to-Bob distance in LOS & NLOS to assess end-to-end performance. Our results are shown in Figure 10 and Figure 11, confirming that Orthcatter performs best.

BER. We vary the communication distance from 0.5m to 20m and show the BER under LOS&NLOS deployments in Figure 10(a) and Figure 11(a). As shown in Figure 10(a), our BER is around 0.1 even when the Tag-to-Bob distance is 6m. It is outstanding because the BER of [22] increases to 1 under the same setting, and that of [23] is over 0.1 even for 2m Tag-to-Bob distance. The side-band RapidRider can maintain its BER below 0.1 only when Bob is less than 7m from Tag. Orthcatter also outperforms them in NLOS.

Throughput. In terms of throughput, neither [22], [23], nor [31] can match our Orthcatter (c.f. Figure 10(b) and Figure 11(b)). Specifically, the maximum throughput in Orthcatter is 248kbps, bigger than 237kbps in RapidRider, and 40kbps in [22], and 54kbps in [23]. There are two main reasons for these results. First, the interference cancellation is conducted before decoding, avoiding the redundant coding method employed by prior in-band works [22, 23]. Second, although Orthcatter and RapidRider conduct symbol-level modulation, Orthcatter experiences a smaller BER and thus better throughput.

Laboratory deployment. We further test Orthcatter in a laboratory to show how it works in a multipath-rich environment shown in Figure 9(a). Figure 9(b) shows that Orthcatter is robust to the multipath effect. Specifically, Orthcatter can maintain its throughput over 100kbps within the room of 65m^2. In position C, the BER is 0.14, similar to the LOS performance. In position D where the steel shelf blocks the direct link between Tag and Bob, our BER is 0.12 similar to the NLOS one. The reason is that our backscatter signal is still an OFDM signal armed with the cyclic prefix that can

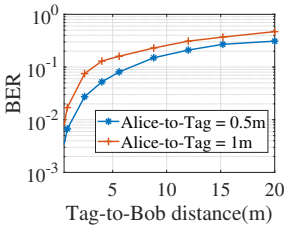

(a) BER

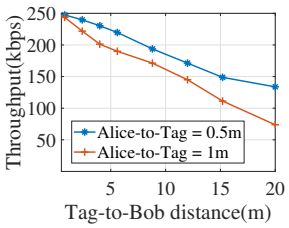

(b) Throughput

Figure 10: Orthcatter's performance in LOS.

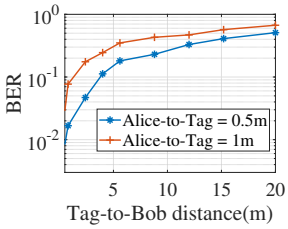

(a) BER

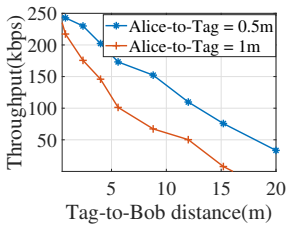

(b) Throughput

Figure 11: Orthcatter's performance in NLOS.

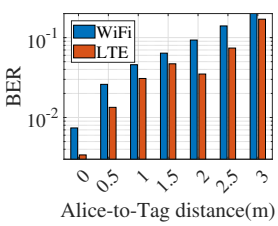

(a) Different exciter types

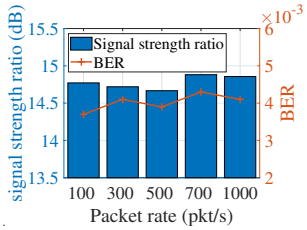

(b) Different packet rates

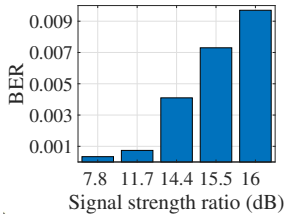

(c) Different signal strength ratios

Figure 12: Orthcatter's performance under different excitation types and packet rates and signal strength ratios.

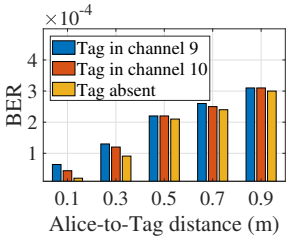

Figure 13: Impact of Orthcatter on the ambient WiFi.

cope with this effect. In addition, the extracted backscatter OFDM symbol after the interference cancellation process also has the pilot subcarriers, which can correct the phase error introduced by the wireless channel.

5.3 Micro Benchmarks

In order to confirm the applicability of Orthcatter to various exciters and deployments, we change Alice's signal type and packet rate and the spatial deployment of Tag. The results show that when the signal strength ratio between the original and backscatter signal is 7.8dB, its BER goes to as low as 3.4×10^{-4}, which is 59× better than the minimal BER of the side-band backscatter system RapidRider [31].

Impact of Alice-to-Tag distance and exciter type. We demonstrate that Orthcatter can work with longer Alice-to-Tag distance and other types of OFDM exciters besides WiFi. In our experiment, the exciter is the down-link LTE signal with a bandwidth of 1.4MHz and 128 subcarriers (72 data subcarriers and 56 null subcarriers). We set the Alice-to-Bob distance to 3m and put Tag in between. As shown in 12(a), the BER is smaller under the LTE exciter. This is because an LTE symbol contains more subcarriers, making it easier for Bob to perform the quasi-orthogonal interference cancellation and decoding. Furthermore, since the CP of an LTE OFDM symbol is far longer than that of WiFi, the tag working with LTE exciters can synchronize with Alice at a farther position. It is worth mentioning that the BER under the LTE exciter of a 1m Alice-to-Tag distance is similar to such BER of a 2m Alice-to-Tag distance. That said, when the Tag is within 2m from Alice, the synchronization error would hardly impact the tag data decoding. This is much better than prior works whose Alice-to-Tag distance is restricted to within 1m [9, 27, 28, 31, 37]. Besides, even with 3m Alice-to-Tag distance, the backscatter communication is still feasible.

Impact of Alice's packet rate. We here increase Alice's packet rate from 100pkt/s to 1000pkt/s and depict our results in Figure 12(b). We set both the Alice-to-Tag distance and the Tag-to-Bob distance at 0.5m in this experiment. The results show that changing excitation rates hardly has impact on the signal strength ratio and BER.

Impact of signal strength ratio. Since the original and backscatter signals are mixed on the receiver side, an important factor affecting our decoding is the signal strength ratio between these signals. We test its influence here and show the results in Figure 12(c). To this end, we should measure the signal strength ratio. This is actual value that would be shown in the x axis. In order to accurately measure the ratio, we replace the wide-band OFDM excitation signal with a narrow-band sine wave, enabling measurement of the narrow-band excitation signal and the narrow-band backscatter signal in the WiFi band. Note that we do not use this ratio for decoding, but use the estimation from null subcarriers (recall Figure 4) instead. We first change the relative positions among Alice, Tag, and Bob to get different signal strength ratios. Second, for each deployment, we ask Alice to generate a sine wave whose frequency spectrum has no overlap with the side-band backscatter one. Hence, we can receive the original and backscatter signals separately and compute their received signal strength. For the testing, we ask Alice to emit the OFDM WiFi signal to test Orthcatter's performance under the measured signal strength ratios. From Figure 12(c),

we have two observations: 1) When the signal strength ratio is 7.8dB, i.e., the original signal strength is 6× higher than backscatter one, the BER of Orthcatter is 3.4×10^{-4}, which is 59× better than the minimal BER of RapidRider. 2) Even when the ratio is 16dB, i.e., 40×, Orthcatter can still keep its BER below 10^{-2}. This demonstrates that Orthcatter can be deployed under diverse settings.

5.4 Coexist with ambient WiFi

We finally evaluate whether our backscatter transmission would impact the ambient WiFi traffics including both the in-band excitation signal (Alice) and an adjacent WiFi signal. We fix the Tag-to-Bob distance at 0.5m and vary the Alice-to-Tag distance. We here use two adjacent channels for the excitation signal (channel 9) and another WiFi signal (channel 10), respectively. Note that we focus on the encoded data before passing through the convolutional decoder because we need to acquire the quasi-orthogonal codewords utilized for the decoding. That said, the actual BER of the excitation signal would be lower due to the convolutional decoder. As shown in Figure 13, Tag would slightly degrade the in-band and side-band WiFi transmission. Consider the worst case where Tag is 0.1m from the exciter, the BER is increased by 4.4×10^{-5}. This increment is small and would be reduced by the convolutional decoder. Moreover, the impact nearly disappears when the distance exceeds 0.5m because of the greatly dropped backscatter signal strength. Therefore, our backscatter transmission hardly harms the ambient WiFi.

6 Discussion

Supporting Multiple tags. In this paper, we primarily focus on improving the point-to-point physical-layer backscatter transmission performance. However, Orthcatter can be expanded to support the access of multiple tags by adopting the MAC layer protocols like TDMA or Aloha.

Commercial receiver. Since tag data is decoded from the frequency-domain OFDM symbol, any OFDM receiver that converts the received signal to the frequency domain can work with Orthcatter. This means that our work has the potential for the commercial applications. However, Orthcatter is not fully compatible with commercial devices that would treat the weaker backscatter signal as noise and neglect it and do not provide access to the received encoded OFDM symbol. We hope that future commercial devices could grant more access to PHY information to make our Orthcatter applicable.

7 Related work

The related work can be classified into the side-band and in-band backscatter systems.

Side-band backscatter systems. Hitchhike [35], FreeRider [36], and MOXcatter [37] are side-band WiFi backscatter systems. They utilize the codeword translation, which embeds tag data by transforming the original codeword into another valid codeword. By avoiding the original signal, these works provide tens of kbps throughput. RapidRider [31] and STScatter [33] design OFDM backscatter and utilize the phase of the backscatter symbol to convey their data. This way, their data is embedded at the single-symbol rate, and their throughput is hundreds of kbps. In addition, PLoRa [29] focuses on the LoRa exciter and embed tag data over the initial frequency of the LoRa signal. LScatter [9] frequency shifts the LTE signal and embeds tag data over its phase.

In-band backscatter systems. Here the backscatter communication is completed in the same channel as the excitation to save the spectrum resource. [22] and [23] embed their data through phase modulation like RapidRider [31] and STScatter [33], yet only has a tens of kbps throughput. [26] and [20] respectively embed their message over ambient TV and WiFi signal amplitude and only provide throughput of several kbps. Aloba [15] conducts LoRa modulation through OOK instead of frequency modulation and has a limited communication range of only $1/3$ of PLoRa [29]. The performance of these in-band backscatter systems is incomparable to the side-band ones because they cannot cope with interference of the excitation signal effectively. Superior to them, our Orthcatter can cancel the interference and achieve even better performance than some side-band works.

8 Conclusion

We have designed and implemented Orthcatter, a novel in-band backscatter system that achieves reliable and high throughput communication while saving spectrum resources. The key innovation lies in the designed over-the-air code division technique that constructs the quasi-orthogonal codewords in the backscatter signal from the original excitation signal passively. This technique enables the in-band interference cancellation on the receiver. Our extensive field studies show that Orthcatter experiences 10^{-4} BER and 248kbps throughput, respectively 300× and 4.6× better than the state-of-the-art in-band system [23]. And it outperforms the side-band system like RapidRider [31] in some settings. Orthcatter can efficiently work under diverse practical scenarios, and would benefit a wide range of future backscatter applications.

9 Acknowledgements

This work was supported in part by National Natural Science Foundation of China under Grant No. 62271055, 62171296, 62122095, 62341201 and 62072472, and by Beijing Natural Science Foundation under Grant No. 4242002, and by a grant from the Guoqiang Institute, Tsinghua University.

References

[1] Adg902 rf switch. https://www.analog.com/media/en/technical-documentation/data-sheets/ADG901-902.pdf.

[2] Adg904 rf switch. https://www.analog.com/media/en/technical-documentation/data-sheets/ADG904.pdf.

[3] Lt5534 detector. https://www.analog.com/media/en/technical-documentation/data-sheets/5534fc.pdf/.

[4] Lte protocol. https://www.3gpp.org/dynareport?code=36-series.html/.

[5] Lte toolbox. https://ww2.mathworks.cn/help/lte/.

[6] Wifi protocol. https://www.tutorialspoint.com/wi-fi/wifi_access_protocols.html/.

[7] Ali Abedi, Farzan Dehbashi, Mohammad Hossein Mazaheri, Omid Abari, and Tim Brecht. Witag: Seamless wifi backscatter communication. In *Proceedings of the ACM SIGCOMM*, page 240–252, 2020.

[8] Bastian Bloessl, Michele Segata, Christoph Sommer, and Falko Dressler. An ieee 802.11a/g/p ofdm receiver for gnu radio. page 9–16, 2013.

[9] Zicheng Chi, Xin Liu, Wei Wang, Yao Yao, and Ting Zhu. Leveraging ambient lte traffic for ubiquitous passive communication. In *Proceedings of the ACM SIGCOMM*, pages 172–185, 2020.

[10] Huixin Dong, Yirong Xie, Xianan Zhang, Wei Wang, Xinyu Zhang, and He Jianhua. Gpsmirror: Expanding accurate gps positioning to shadowed and indoor regions with backscatter. In *Proceedings of the ACM MobiCom*, 2023.

[11] Caihui Du, Jiahao Liu, Shuai Wang, Rongrong Zhang, Wei Gong, and Jihong Yu. Timespan-based backscatter using a single cots receiver. In *Proceeding of the ACM MobiSys*, pages 450–461, 2023.

[12] Manideep Dunna, Miao Meng, Po-Han Wang, Chi Zhang, Patrick Mercier, and Dinesh Bharadia. SyncScatter: Enabling WiFi like synchronization and range for WiFi backscatter communication. In *Proceeding of the USENIX NSDI*, pages 923–937, 2021.

[13] Yalda Edalat, Katia Obraczka, and Bahador Amiri. A machine learning approach for dynamic control of rts/cts in wlans. In *proceedings of the EAI MobiQuitous*, pages 432–442, 2018.

[14] Xiuzhen Guo, Yuan He, Zihao Yu, Jiacheng Zhang, Yunhao Liu, and Longfei Shangguan. Rf-transformer: A unified backscatter radio hardware abstraction. In *Proceedings of the ACM MobiCom*, page 446–458, 2022.

[15] Xiuzhen Guo, Longfei Shangguan, Yuan He, Jia Zhang, Haotian Jiang, Awais Ahmad Siddiqi, and Yunhao Liu. Efficient ambient lora backscatter with on-off keying modulation. *IEEE/ACM Transactions on Networking*, 30(2):641–654, 2021.

[16] Roger Pierre Fabris Hoefel. Ieee wlans: 802.11, 802.11e mac and 802.11a, 802.11b, 802.11g phy cross layer link budget model for cell coverage estimation. In *Proceeding of the IEEE CCECE*, pages 1877–1882, 2008.

[17] Youjun Hu. Fourier analysis. 1970.

[18] Andrew H Jazwinski. Adaptive filtering. *Automatica*, 5(4):475–485, 1969.

[19] Jinyan Jiang, Zhenqiang Xu, Fan Dang, and Jiliang Wang. Long-range ambient lora backscatter with parallel decoding. In *Proceedings of the ACM MobiCom*, pages 684–696, 2021.

[20] Bryce Kellogg, Aaron Parks, Shyamnath Gollakota, Joshua R Smith, and David Wetherall. Wi-fi backscatter: Internet connectivity for rf-powered devices. In *Proceedings of the ACM SIGCOMM*, pages 607–618, 2014.

[21] Bryce Kellogg, Vamsi Talla, Shyamnath Gollakota, and Joshua R Smith. Passive wi-fi: Bringing low power to wi-fi transmissions. In *Proceeding of tbe USENIX NSDI*, pages 151–164, 2016.

[22] Taekyung Kim and Wonjun Lee. Exploiting residual channel for implicit wi-fi backscatter networks. In *Proceeding of the IEEE INFOCOM*, pages 1268–1276, 2018.

[23] Taekyung Kim and Wonjun Lee. Channel independent wi-fi backscatter networks. In *Proceeding of the IEEE INFOCOM*, pages 262–270, 2019.

[24] Jeongkeun Lee, Wonho Kim, Sung-Ju Lee, Daehyung Jo, Jiho Ryu, Taekyoung Kwon, and Yanghee Choi. An experimental study on the capture effect in 802.11a networks. In *Proceedings of the ACM WiNTECH*, page 19–26, 2007.

[25] Li Erran Li, Kun Tan, Harish Viswanathan, Ying Xu, and Yang Richard Yang. Retransmission $\neq$ repeat: simple retransmission permutation can resolve overlapping channel collisions. In *Proceedings of the ACM MobiCom*, page 281–292, 2010.

[26] Vincent Liu, Aaron Parks, Vamsi Talla, Shyamnath Gollakota, David Wetherall, and Joshua R Smith. Ambient backscatter: Wireless communication out of thin air. In *Proceedings of the ACM SIGCOMM*, pages 39–50, 2013.

[27] Xin Liu, Zicheng Chi, Wei Wang, Yao Yao, Pei Hao, and Ting Zhu. Verification and redesign of ofdm backscatter. In *Proceeding of the USENIX NSDI*, pages 939–953, 2021.

[28] Xin Na, Xiuzhen Guo, Zihao Yu, Jia Zhang, Yuan He, and Yunhao Liu. Leggiero: Analog wifi backscatter with payload transparency. In *Proceedings of the ACM MobiSys*, page 436–449, New York, NY, USA, 2023.

[29] Yao Peng, Longfei Shangguan, Yue Hu, Yujie Qian, Xianshang Lin, Xiaojiang Chen, Dingyi Fang, and Kyle Jamieson. Plora: A passive long-range data network from ambient lora transmissions. In *Proceedings of the ACM SIGCOMM*, pages 147–160, 2018.

[30] Mohammed Saad Talib, Burairah Hussin, and Aslinda Hassan. Converging vanet with vehicular cloud networks to reduce the traffic congestions: A review. *Int. J. Appl. Eng. Res*, 12(21):10646–10654, 2017.

[31] Qiwei Wang, Si Chen, Jia Zhao, and Wei Gong. Rapidrider: Efficient wifi backscatter with uncontrolled ambient signals. In *Proceeding of the IEEE INFOCOM*, pages 1–10, 2021.

[32] Chenren Xu and Pengyu Zhang. Open-source software and hardware platforms for building backscatter systems. *GetMobile: Mobile Computing and Communications*, 23(1):16–20, 2019.

[33] Yifan Yang and Wei Gong. Universal space-time stream backscatter with ambient wifi. In *proceeding of the IEEE PerCom*, pages 101–110. IEEE, 2022.

[34] Jihong Yu, Caihui Du, Jiahao Liu, Rongrong Zhang, and Shuai Wang. Subscatter: Subcarrier-level ofdm backscatter. In *Proceeding of the IEEE INFOCOM*, pages 1–10, 2023.

[35] Pengyu Zhang, Dinesh Bharadia, Kiran Joshi, and Sachin Katti. Hitchhike: Practical backscatter using commodity wifi. In *Proceedings of the ACM SenSys*, pages 259–271, 2016.

[36] Pengyu Zhang, Colleen Josephson, Dinesh Bharadia, and Sachin Katti. Freerider: Backscatter communication using commodity radios. In *Proceedings of the ACM CoNEXT*, pages 389–401, 2017.

[37] Jia Zhao, Wei Gong, and Jiangchuan Liu. Spatial stream backscatter using commodity wifi. In *Proceedings of the ACM MobiSys*, pages 191–203, 2018.

[38] Renjie Zhao, Fengyuan Zhu, Yuda Feng, Siyuan Peng, Xiaohua Tian, Hui Yu, and Xinbing Wang. Ofdma-enabled wi-fi backscatter. In *The 25th Annual International Conference on Mobile Computing and Networking*, pages 1–15, 2019.

[39] Fengyuan Zhu, Yuda Feng, Qianru Li, Xiaohua Tian, and Xinbing Wang. Digiscatter: Efficiently prototyping large-scale ofdma backscatter networks. In *Proceedings of the ACM MobiSys*, page 42–53, New York, NY, USA, 2020.